

pubs.acs.org/acsapm Article

# Tuning the Properties of Nanocomposites by Trapping Them in Deep Metastable States

Zhengping Zhou,\* Vera Bocharova, Rajeev Kumar, Anne-Caroline Genix, Bobby Carroll, Subarna Samanta, Ivan Popov, Amanda Young-Gonzales, Alexander Kisliuk, Seung Pyo Jeong, Jan Ilavsky, and Alexei P. Sokolov\*



Cite This: ACS Appl. Polym. Mater. 2022, 4, 3174–3182



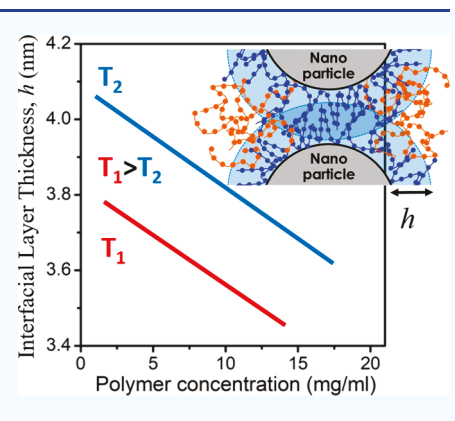
**ACCESS** 

Metrics & More

Article Recommendations

s Supporting Information

ABSTRACT: The interfacial region formed in a polymer matrix around nanoparticles (NPs) controls many macroscopic properties of polymer nanocomposites (PNCs). However, understanding the factors controlling the structure and properties of the interfacial region remains a challenge. We demonstrated that the initial trapping of polymer chains at surfaces of NPs in solution strongly affects the macroscopic properties of PNCs. The most surprising result is that the differences in properties of PNCs persist even after an extremely long thermal annealing time. We ascribe the observed changes to the formation of an interfacial layer that is trapped in a deep metastable state already in solution. Furthermore, the presented analysis suggests that the PNC equilibration time is defined by the chain desorption time that can be extremely long and, in some cases, even not accessible on a reasonable experimental time scale. These results highlight the importance of polymer solution concentrations on the formation of an interfacial layer and the macroscopic properties of PNCs.



KEYWORDS: Polymer nanocomposites, photon correlation spectroscopy, interfacial layer model, Brillouin light scattering, SCFT calculations

#### **■ INTRODUCTION**

Polymer nanocomposites (PNCs) are used in many advanced technologies. Their broad use is due to their lightweight, easy processability, and possibility to tune their properties. 1-8 Addition of nanoparticles (NPs) to polymers leads to the formation of an interfacial region of a few nanometer thickness around NPs. The properties of the interfacial region are significantly different from those of a neat polymer, which provides an opportunity to tune the macroscopic properties of PNCs by controlling interfacial regions. In general, macroscopic properties of PNCs are ascribed to the large volume fraction of the interfacial regions due to the relatively high surface area of NPs. 9-11 However, despite the significant recent progress in studies of the interfacial region, 10,12-24 a fundamental understanding of parameters controlling the interfacial layer structure and properties remains limited, which hinders the rational design of PNCs with desired properties.

Recent developments in PNCs have demonstrated that interfacial layer properties depend on many factors, including the NP size and loading, temperature, polymer chain rigidity and molecular weight, polymer—NP interactions, and chain stretching. <sup>10,16–23,25</sup> It is now well established that the thickness of the interfacial layer increases with a decrease in the NP surface curvature (an increase in the size), <sup>25</sup> with an increase in polymer rigidity, and upon cooling. <sup>19</sup> It has also

been reported that the preparation conditions could lead to variations in macroscopic properties. 26,27 For instance, earlier studies revealed that solvents used during preparation affect the macroscopic properties of PNCs. 26,27 The results suggest that the initial formation of an interfacial layer occurring in a solution could play an important role in determining PNCs' macroscopic properties. While substantial research of PNCs has been done to date, we still lack an understanding of how we can control the formation of an interfacial region in a solution and how the initially formed interfacial region affects the macroscopic properties of PNCs.

In this study, we analyze the influence of the solvent content used in the PNC preparation on the interfacial layer and macroscopic mechanical properties of PNCs. Use of the same polymer and the same NP loading should result in PNCs with the same properties. However, our analysis revealed that mechanical and dielectric properties of the PNCs depend on the solvent concentration during the preparation, and the

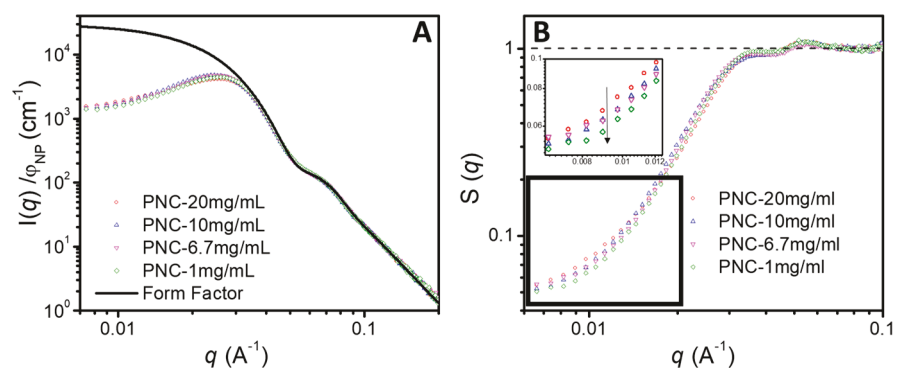
Received: November 16, 2021 Accepted: March 29, 2022 Published: April 12, 2022





Table 1. Characteristics of P2VP and PNCs

samples	volume fraction of NPs (%)	d <sub>IPS</sub> (eq 2, nm)	T <sub>g</sub> (BDS K)	T <sub>g</sub> (DSC, K)	density (kg/m³)	longitudinal sound velocities (m/s)	longitudinal modulus (M, GPa)	$\begin{array}{c} \text{transverse} \\ \text{sound velocities} \\ \text{(m/s)} \end{array}$	shear modulus ( <i>G</i> , GPa)	bulk modulus (K, GPa)
P2VP	N/A	N/A	369.0	372.4	$1197 \pm 6.5$	$2578.4 \pm 30.9$	$8.0 \pm 0.2$	$1314.8 \pm 20.8$	$2.1 \pm 0.1$	$5.2 \pm 0.3$
PNC-20 mg/mL	$23.6 \pm 0.4$	4.9	369.2	375.3	$1415 \pm 3.0$	$2827.8 \pm 48.2$	$11.3 \pm 0.4$	$1567.4 \pm 46.4$	$3.5 \pm 0.2$	$6.7 \pm 0.5$
PNC-10 mg/mL	$24.1 \pm 0.6$	4.7	369.0	375.2	$1454 \pm 8$	$2861.4 \pm 36.8$	$11.9 \pm 0.4$	$1551.3 \pm 34$	$3.5 \pm 0.2$	$7.2 \pm 0.4$
PNC-6.7 mg/mL	$23.7 \pm 1.1$	4.8	365.7	374.1	$1451 \pm 4.5$	$2887.2 \pm 37.0$	$12.1 \pm 0.3$	$1554.1 \pm 37.0$	$3.5 \pm 0.2$	$7.4 \pm 0.4$
PNC-1 mg/mL	$23.2 \pm 0.9$	5.0	366.6	370.2	$1453\pm19$	$2913.9 \pm 43.6$	$12.3 \pm 0.5$	$1608.8 \pm 50.2$	$3.8\pm0.3$	$7.3 \pm 0.6$



**Figure 1.** (A) SAXS spectra of PNCs after subtraction of the pure polymer contribution and normalized to the  $SiO_2$  NP volume fraction. The form factor (P(q)) was measured using a dilute (0.7 vol %) solution of  $SiO_2$  NPs in ethanol. (B) Structure factors for all herein studied PNCs. (Inset) Zoomed structure factors of PNCs in the low-q range show a systematic decrease in dilution of polymer solution. The error bars do not exceed 1%.

difference remains even after very long annealing of the samples (annealing time is  $\sim 10^{10}$  times that of the segmental relaxation time). We demonstrate that the differences in macroscopic properties are related to the changes in the interfacial layer that persist even after a long annealing time. These results suggest that PNCs during preparation are trapped in deep metastable states. We suggest that the characteristic equilibration time of PNCs might be controlled by the chain desorption. The latter might be longer than any reasonable annealing time used in practical applications. These results suggest a rather simple way to tune the macroscopic properties of PNCs by trapping them in different deep metastable states already in a solution, for example, by changing solvents, solution concentrations, and so forth.

#### **■** RESULTS

Table 1 summarizes the properties of various PNCs studied in this work. We used poly(2-vinyl pyridine) (P2VP) with a molecular weight of 400,000 g/mol and silica NPs with a radius  $R_{\rm NP}$  = 8.0 nm loaded into the polymer matrix at  $\varphi_{\rm NP}$  ~ 24 vol %. The same amounts of polymer and NPs were dissolved in various amounts of ethanol and mixed for at least 12 h. Then, PNCs were formed by evaporating the solvent. The formed PNCs were then dried in a vacuum oven at 373 K for 2 days to remove any residual solvent and adsorbed water. Additional thermal treatment for the samples was applied before experimental characterization (see Materials and Methods sections for details). The samples were named according to the weight of polymer per mL of solvent, for example, PNC-20 mg/mL was prepared from solution containing 20 mg of polymer per mL. A detailed description of the sample preparation is presented in the Materials and Methods section. The averaged interparticle spacing between the NPs  $(d_{IPS})$  is computed using their volume fraction in the PNCs (see the Materials and Methods section for details). Similarly, we have estimated the average surface-to-surface

distance  $(d_{NP})$  of SiO<sub>2</sub> NPs in solutions using the volume fraction of NPs in solution. These estimates and estimates of the polymer radius of gyration  $(R_g)$  in solution are presented in the Supporting Information. In particular, composites were prepared in ethanol, which is a good solvent for P2VP, and  $R_{\sigma}$ of the polymer was calculated to be ~35.0 nm, providing estimates of the critical concentration for crossover from the dilute to semidilute regime to be ~3.5 mg/mL. For the most diluted solution of 1 mg/mL, the  $d_{\rm NP}$  was estimated to be ~183 nm, which is more than 2 times larger than  $2R_e$ . However,  $d_{NP}$  decreases to ~57 nm in the most concentrated solution of 20 mg/mL, that is, it becomes smaller than  $2R_g$ . To verify the effect of solvent concentrations on the polymer-NP interactions, we used photon correlation spectroscopy (PCS) to determine the effective size of NPs in polymer solutions (Figure S1 and Table S1). The mean radius of NPs in the 1 mg/mL sample is ~39 nm (Table S1), comparable to  $\sim R_{\rm NP}$  +  $R_{\sigma}^{28}$ . However, this size increases ~3-4 times in a concentrated solution of 20 mg/mL (Table S1), indicating the chain-mediated aggregation of NPs. To verify stability of these aggregates, we diluted the concentrated 20 mg/mL sample down to 1 mg/mL. The mean radius of NPs decreases to 47.5 nm, but it remains larger than that of PNC-1 mg/mL, suggesting that the chain-mediated aggregation in PNC solutions can be relatively stable.

The microstructure of PNCs and the dispersion of SiO<sub>2</sub> NPs were analyzed using small-angle X-ray scattering (SAXS). The SAXS spectra show a well-defined repulsive interaction peak in the low-q range of  $\sim 0.024-0.026$  Å<sup>-1</sup> (Figure 1A), which suggests good NP dispersion in all the samples. For the particular case of a system with monodisperse spherical particles, the scattering intensity is described as  $I(q) \propto \varphi_{\rm NP}P(q)S(q)$ , where P(q) is the form factor of a spherical particle and S(q) is the structural factor presenting position correlations between particles. P(q) is taken as I(q) of the diluted NP suspension (Figure 1A). P(q) was used to estimate

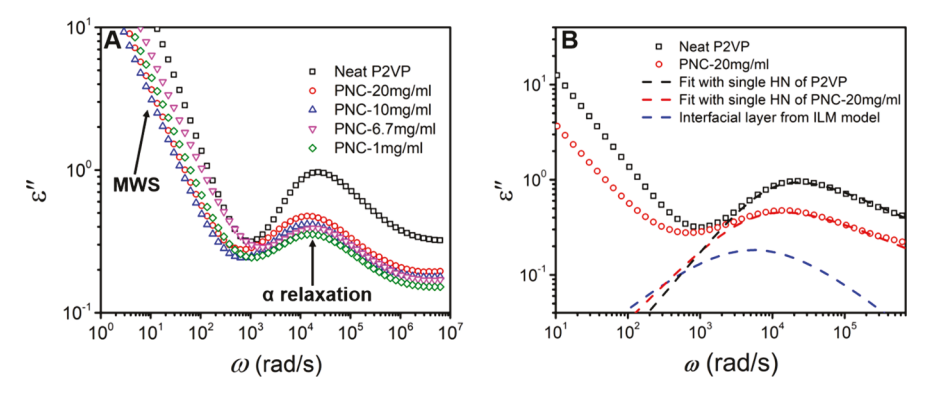


Figure 2. (A) Loss spectra ( $\varepsilon''(\omega)$ ) collected at 413 K for the neat P2VP and PNCs with different polymer solution concentrations: neat P2VP (black squares), 20 mg/mL (red circles), 10 mg/mL (blue upper triangles), 6.7 mg/mL (magenta down triangles), and 1 mg/mL (olive diamonds). (B) Comparison of the dielectric loss spectra of neat P2VP and PNC (plain circles). The response from the interfacial layer process (blue-dashed line) is shown for the nanocomposite sample, while the single-Havriliak-Negami (HN) functions for both the PNC (red-dashed line) and the polymer (black-dashed line) are presented.

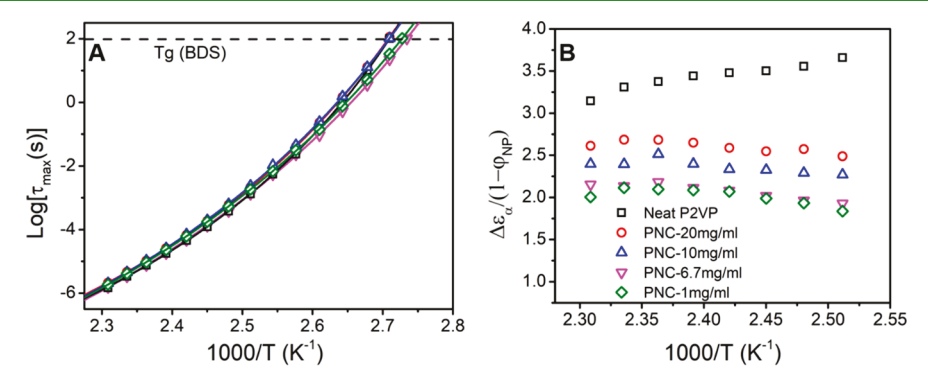


Figure 3. (A) Temperature dependence of the segmental relaxation times estimated from the peak position for P2VP and PNCs and their fits using the VFT equation. (B) Temperature dependence of the total dielectric amplitude of P2VP and PNCs with different polymer solution concentrations: neat P2VP (black squares), 20 mg/mL (red circles), 10 mg/mL (blue upper triangles), 6.7 mg/mL (magenta down triangles), and 1 mg/mL (olive diamonds).

 $S(q) \sim I(q)/P(q)$  of studied PNCs (Figure 1B). Detailed analysis of S(q) revealed a systematic decrease in intensity at low q (region  $\sim 0.006-0.015$  A<sup>-1</sup>) with a decrease of the polymer concentration in solutions (Figure 1Binset). The decrease in the intensity is confirmed by ultrasmall angle X-ray scattering (USAXS) measurements, presented in Figure S13 in the Supporting Information. This result suggests that even after a long annealing time, the static structure of PNCs still depends on preparation conditions. In contrast, differential scanning calorimetry (DSC) results revealed no systematic change in  $T_g$  (Table 1, Figures S2 and S3).

To explore the effect of polymer concentrations on the segmental dynamics in PNCs, we used broadband dielectric spectroscopy (BDS) in a broad frequency range of  $10^{-2}$  to  $10^{7}$ Hz. The dielectric loss spectra  $\varepsilon''(\omega)$  exhibit a peak associated with the polymer segmental relaxation (Figure 2A). Compared to the dielectric loss spectra of neat P2VP, the peak in the spectra of PNCs is shifted slightly in frequency but shows a significant decrease in the amplitude. The presence of silica NPs resulted also in the additional Maxwell-Wagner-Sillar's polarization and a decrease in conductivity. All these changes are consistent with previous BDS studies of PNCs. 16-20,25,29

Analysis of the BDS spectra (Figure 2A) reveals that the magnitude of the segmental peak gradually decreases with a decrease of the polymer solution concentrations, while the position of the peak barely changes. To obtain more insights,

we first fitted the dielectric permittivity spectra to a single HN function plus conductivity

$$\varepsilon^*(\omega) = \varepsilon_{\infty} + \frac{\Delta \varepsilon}{\left[1 + (i\omega \tau_{HN})^{\alpha}\right]^{\gamma}} - i \frac{\sigma}{\varepsilon_0 \omega}$$

where  $\varepsilon^*(\omega)$ ,  $\varepsilon_{\infty}$ ,  $\omega$ ,  $\varepsilon_0$ , and  $\sigma$  are the complex dielectric function of the nanocomposites, the dielectric constant at infinite frequency, the angular frequency, the vacuum permittivity, and the dc conductivity, respectively;  $\Delta \varepsilon$  is the dielectric amplitude of the relaxation process, while  $au_{
m HN}$  is the HN relaxation time; and  $\alpha$  and  $\gamma$  are the two shape parameters of the HN function that represent the stretching and asymmetry of the relaxation peak. Figure 2B presents examples of the fit with one-HN function for the neat polymer and PNC-20 mg/mL. The segmental relaxation time  $(\tau_{max})$ obtained from the one-HN function fittings as  $\tau_{\rm max}$  = 1/  $(2\pi f_{\text{max}})$  is plotted in Figure 3A, where  $f_{\text{max}}$  is the frequency representing the peak in the  $\varepsilon''$  function. Such an analysis based on single-HN peak relaxation times reveals no significant dependence on the polymer solution concentration. In order to demonstrate this in a quantitative manner, the glass-transition temperature  $(T_g)$  was estimated by fitting the temperature dependence of the segmental relaxation times to the Vogel-Fulcher–Tammann (VFT) equation,  $\tau_{\alpha} = \tau_0 \exp\left(-\frac{B}{T - T_0}\right)$ 

where  $\tau_0$ , B, and  $T_0$  are the fitting parameters and  $T_g$  can be

defined as the temperature at which  $\tau_{\alpha}$  = 100 s (Figure 3A). In agreement with the DSC data, the estimated  $T_{\rm g}$  values from BDS (Table 1) did not change significantly with polymer solution concentrations. In addition, the fittings using the HN function provided an estimate for the dielectric amplitude of the segmental relaxation in PNCs  $(\Delta arepsilon_{ ext{PNC}})$  and the neat polymer ( $\Delta \varepsilon_{\text{neat}}$ ). The dielectric strength of the segmental relaxation in PNCs decreased stronger than expected from the polymer volume fraction (Figure 3B). Surprisingly,  $\Delta \varepsilon_{PNC}$ monotonically decreased with the dilution of polymer solution from 20 to 1 mg/mL (Figure 3B). Because all PNCs had the same NP loading of ~24 vol %, this decrease in  $\Delta \varepsilon_{\rm PNC}$  can be associated with the decrease of the bulk-like polymer fraction and the increase in the interfacial layer fraction. We also note that the dielectric strength in all PNCs decreases upon cooling, while the dielectric strength increases in the neat polymer (Figure 3B). This effect has been observed in other studies 19,30 and is ascribed to the increase of the interfacial layer thickness on cooling.

To examine the PNC's mechanical properties, we used Brillouin light scattering (BLS) and measured all the samples at room temperature in a symmetric scattering geometry. Figure S4 presents the BLS spectra of the neat polymer and PNCs with the longitudinal modes (LM) in the main figure and the transverse modes (TM) in the inset. In comparison with the neat polymer, both LM and TM spectra show a clear shift of the Brillouin peaks toward higher phonon frequencies, indicating an increase in the mechanical moduli of PNCs, similar to the previous reports. 9,31,32 To evaluate their mechanical moduli, a damped-harmonic oscillator function was employed to fit the spectra and to estimate the peak frequency for the longitudinal  $(\nu_{\rm L})$  and transverse  $(\nu_{\rm T})$ Brillouin modes.<sup>33</sup> These peak frequencies were used to calculate sound velocities using the equation valid for 90° symmetric scattering geometry, <sup>32</sup>  $V_{\rm L,T} = \lambda \nu_{\rm L,T} / \sqrt{2}$  , where  $V_{\rm L}$ and  $V_{\rm T}$  are the longitudinal and transverse sound velocity, respectively, and  $\lambda = 532$  nm is the laser wavelength.

The longitudinal  $(M = \rho V_L^2)$ , shear  $(G = \rho V_T^2)$ , and bulk (K = M - 4/3G) moduli (Table 1) were calculated using the obtained sound velocities (here  $\rho$  is the mass density measured by pycnometry). Analysis (Figure 4) reveals that both bulk and shear moduli of PNCs are slightly higher than the values estimated from a Hashin–Shtrikman two-phase model

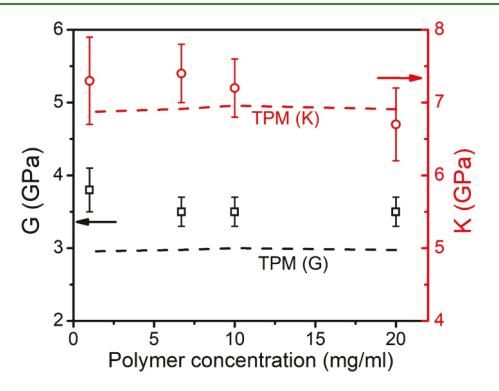


**Figure 4.** Shear (G) and bulk (K) moduli of P2VP/silica nanocomposites prepared from solutions containing varying polymer concentrations. The black- and red-dashed lines represent G and K moduli of PNCs, respectively, that were calculated based on a Hashin–Shtrikman two-phase model (TPM).

(TPM), 34,35 which does not account for the interfacial layer, emphasizing importance of the interfacial layer in the mechanical reinforcement. Details of the TPM model can be found in the Supporting Information. Exception is the bulk modulus of the PNC-20 mg/mL sample, which appears to be smaller than expected from TPM (Figure 4). This result is consistent with earlier studies of molecular weight dependence in these PNCs and is explained by frustration in packing of long chains. 9,16 It is worth noting that both moduli demonstrate a weak dependence on the solution concentration (Figure 4) with the moduli being higher for PNCs prepared from more dilute solutions. This result emphasizes that the initial solution concentration affects the interfacial layer and the macroscopic mechanical properties of PNCs.

#### DISCUSSION

The presented analysis revealed surprising results—static (S(q)), mechanical, and dielectric properties of the model PNCs all exhibit monotonous dependence on the polymer solution concentration. Although some of the changes are not significant, they are especially surprising because all the samples are annealed at T = 423 K (far above  $T_g$ ) for 12 h, which corresponds to  $\sim 10^{10} \tau_{\alpha}$ , with  $\tau_{\alpha} \sim 10^{-6}$  s at T = 433 K (Figure 3A). Despite such a long annealing time, the difference in PNC properties persists. These results suggest the influence of the polymer solution concentration on the formation of an interfacial region during the preparation of PNCs. As demonstrated in our PCS measurements (Figure S1, Table S1), an increase in the polymer concentration leads to the formation of relatively stable polymer-bridged aggregation of NPs. This affects significantly the macroscopic properties of PNCs after the solvent evaporation, and the effect cannot be erased even after long annealing. Apparently, adsorbed chains are trapped in a deep metastable state that cannot be equilibrated even during a rather long annealing protocol.

To better understand the influence of the solution concentration on the interfacial layer, we analyzed the BDS spectra of PNCs using the interfacial layer model (ILM). 10,16-23 Details of the ILM fit of the BDS spectra are presented in the Supporting Information. ILM provides a good description of the BDS spectra (Figure 2B) and estimates the thickness of the interfacial layer  $l_{\mathrm{IL}}$ , the dielectric strength  $(\Delta \varepsilon_{\rm IL})$ , and the characteristic time of segmental relaxation in the interfacial region (Figures 5 and S5). The segmental relaxation time in the interfacial layer is about 1 order slower than that in the bulk-like polymer (Figure S5), consistent with earlier studies. <sup>9,10,16,17,19</sup> The thickness of the interfacial layer clearly increases with a decrease in the polymer solution concentration, while the dielectric strength  $\Delta \varepsilon_{\mathrm{IL}}$  decreases (Figures 5 and S6). The latter indicates much stronger restrictions on segmental fluctuations in the interfacial layer 16,30 for PNCs prepared from more dilute solutions. In other words, use of more dilute solutions leads to the formation of a better packed and thicker interfacial layer. This conclusion is consistent with the density measurements, which also indicate lower density for the samples prepared from more concentrated solutions (Table 1). Most probably, chainmediated aggregates formed in concentrated solutions are difficult to redisperse during the solvent evaporation, which leads to more frustrated chain packing in the interfacial layer surrounding NPs.

Using the obtained volume fraction of the IL and BLS results, both bulk and shear moduli of the interfacial layer were

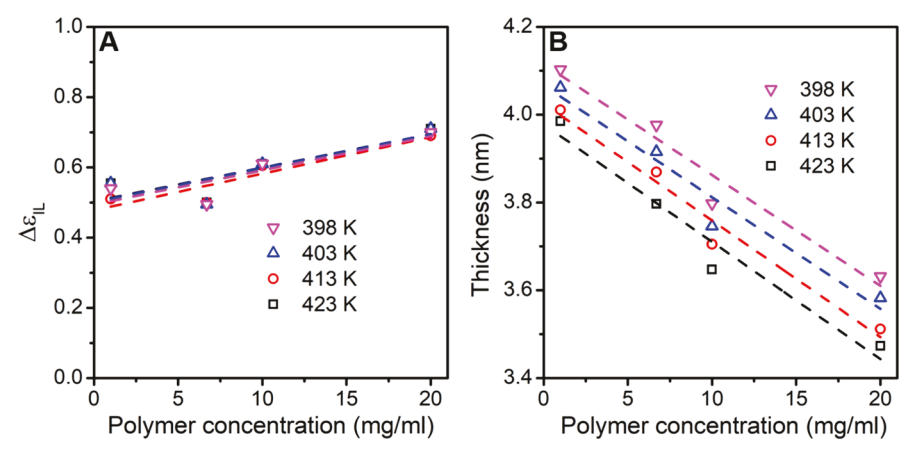
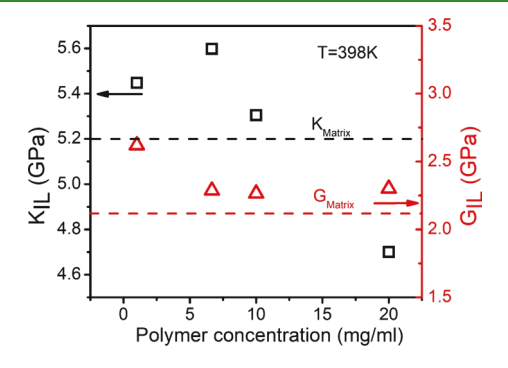


Figure 5. (A) Dielectric strength of IL presented as a function of polymer concentration; and (B) thickness of the interfacial region in the PNCs with the same silica content presented as a function of polymer concentration.

calculated based on ILM for mechanical properties (Figure 6).<sup>36</sup> Detailed calculations are presented in the Supporting



**Figure 6.** Bulk modulus  $(K_{\rm IL})$  and shear modulus  $(G_{\rm IL})$  of the interfacial region in PNCs calculated from the ILM approach. Blackand red-dashed lines represent  $K_{\rm Matrix}$  and  $G_{\rm Matrix}$  moduli of the polymer, respectively.

Information. We selected the volume fraction of IL obtained at a temperature  $T=1.1T_{\rm g}$  ( $T_{\rm g}$  of PNCs) as the closest to the glassy state in our experiments. Only the sample prepared from the highest concentration (20 mg/mL) shows a decrease in the bulk modulus of the interfacial layer (Figure 6). This was observed in earlier studies of high-molecular-weight PNC and was ascribed to frustration of long-chain packing. In all other cases, the analysis revealed an increase in the glassy moduli of the interfacial layer with dilution in polymer

solution. This result is consistent with the conclusion of better chain packing in the interfacial layer made on the basis of the BDS studies. The observed decrease of S(q) at low q (Figure 1B) suggests lower compressibility of PNCs prepared from more dilute solution, consistent with the change in the bulk modulus (Figure 4B). It might also suggest a lower degree of short segment bridging of NPs prepared from less-concentrated solutions.<sup>37</sup>

The differences observed between the interfacial layer moduli for PNCs are likely due to the difference in polymer rearrangement on NPs. To gain more insights into initial chain adsorption on NPs during PNC preparation, we have used a self-consistent field theory (SCFT) based calculations (detailed SCFT calculations are presented in the Supporting Information). For our calculations, the number of polymer chains per NP is fixed with varying polymer solution concentrations (Table S2). The segment and solvent density profiles are obtained by solving the SCFT equations obtained by using the saddle-point approximation. To better illustrate the effect of polymer concentration on the segment density profiles, we divide the segment density profiles into the spatial distributions of the loops, tails, and free chains. Comparing segment density profiles between the most concentrated and the most diluted solutions reveals the chain formation of thinner and thicker interfacial region of PNCs (Figures 7 and S7-S9), respectively.

In the most concentrated polymer solution (Figure 7A), it seems that the loops dominate the segment density profile for chain adsorption. Almost all the loops are adsorbed to NPs to

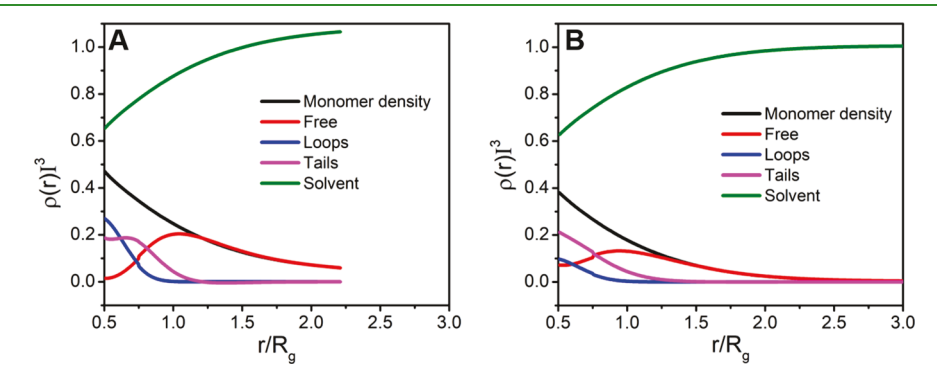
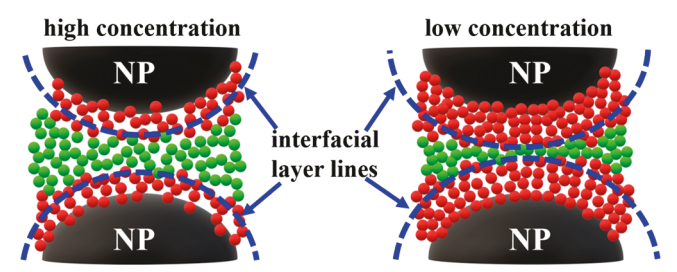


Figure 7. Segment and solvent density profiles near a single NP for (A) concentrated  $(nNR_g^3/V = 137.49)$  and (B) diluted solutions  $(nNR_g^3/V = 6.87)$ . Also, spatial distributions of loops, tails, free chains, and solvents are presented.

form a thin interfacial region with the frustrated chain packing (Scheme 1). As a consequence, the formed initial interfacial

Scheme 1. Proposed Mechanism for Polymer Chain Packing in PNCs with High (Left) and Low (Right) Polymer Concentrations in the Precursor Solution<sup>a</sup>



"The major difference appears in the packing of segments in the interfacial layer (red segments) and the fraction of the bulk-like polymer (green segments).

region restricts the packing of free chains, which leads to a dramatic reduction in free chain segment density close to the NP. The physical adsorption of polymer chains on the NP surface in PNCs has been confirmed in our previous studies. 9,22 The loose polymer packing and lower density in the interfacial region can be explained by the chain confinement between NPs. When the distance between NP surfaces becomes smaller than 2Rg, the polymer loops are strongly confined and induce strong repulsive chain-chain interactions in the formed interfacial region. This interaction leads to a loose packing and a lower volume fraction of the interfacial layer. In addition, in the concentrated solution, a NP must has multiple NP neighbors, which tends to form polymerbridged aggregations evidenced from PCS experiments. This phenomenon is similar to a well-known interference effect<sup>38</sup> that adding more NPs reduces their surface to surface distance, resulting in more overlaps of polymer-layering correlations and less polymer density near a NP surface. 37 On the contrary, in the case of the diluted solution, the distance between NPs becomes much larger than  $2R_{g'}$  and the tails contribute more than the loops to the segment density in nanocomposites (Figure 7B). The tails further propagate to pack better at the interfacial layer in comparisons with the confined loops in the concentrated polymer solution. In addition, the diluted samples have enough non-adsorbed free chains, which can easily penetrate the interfacial region and increase the density.

The presented experimental results and the simulations clearly demonstrate that the initial chain adsorption on NPs during PNC preparation strongly influences the microstructure of the interfacial region and affects mechanical as well as dielectric properties of PNCs. The most surprising result is that even extremely long annealing on a time scale  $\sim \tau_{\alpha} \times 10^{10}$ does not remove the difference in the properties of PNCs. This effect can be explained by a very long time of the chain desorption from NPs and similar to the effect of a very long equilibration time found in the thin supported films. 15 To further verify this point, both P2VP and PNC-20 mg/mL samples were measured at T = 433 K in BDS during a long time of annealing. The characteristic time of the main relaxation process of PNC-20 mg/mL continuously changes with annealing time until  $\sim$ 7 × 10<sup>10</sup>  $\tau_{\alpha}$  ( $\sim$ 20 h), while neat P2VP does not show any significant changes (Figures S10 and S11). This result clearly demonstrates that the PNC remains in

a non-equilibrium state even after a long annealing time, further confirming that the interfacial layer in PNCs is trapped in a deep metastable state already in a polymer solution. It is known that P2VP forms hydrogen bonds with hydroxyl groups on the silica surface and their interaction strength is ~15 kJ/ mol.<sup>28</sup> A single P2VP chain with a molecular weight of 400k should have more than five segments interacting with NP of 8 nm radius (see Section S12 in the Supporting Information for analytical estimates). In this case, the interactions of a chain with a NP will lead to the chain desorption time longer than  $\sim \tau_{\alpha} \times 10^{13}$ . This analysis suggests that the PNC equilibration time is defined by the chain desorption time that can be extremely long and may even be not achievable on any reasonable experimental time scale. These results also suggest that the comparison of PNC data obtained in different laboratories should be taken with caution due to variations in the sample preparation. At the same time, it opens a rather simple way of tuning PNC properties (in a limited range, of course) by changing the way they are prepared.

#### CONCLUSIONS

In summary, through a combination of SAXS, BDS, PCS, and BLS measurements, we have systematically investigated the influence of polymer solution concentrations on dynamic and mechanical properties in P2VP/silica nanocomposites with a constant loading of NPs. Although bulk-like segmental relaxation time and  $T_{\rm g}$  of PNCs appear to be rather insensitive to preparation conditions, the interfacial layer thickness and its mechanical and dielectric properties revealed a significant dependence on the amount of solvent used in the preparation of PNCs. This is consistent with earlier reports on the use of different solvents that strongly influence macroscopic PNC properties. The most surprising result is that even after an extremely long annealing time, the difference in these PNC properties remains.

We suggest that the adsorption of polymer chains to NPs in solution strongly affects the structure, dynamics, and mechanical properties of the interfacial layer and might be a key to tuning the macroscopic properties. Preparing PNC from a rather dilute polymer solution leads to a better packing of chains in the interfacial layer due to a larger amount of free chains and to the formation of a thicker interfacial layer. The existence of the difference between PNC properties even after an extremely long annealing time suggests that the chain desorption time might be the critical equilibration time for PNCs. This time might be not accessible on a usual experimental time scale, leading us to a conclusion that the most of the PNCs are probably studied in their nonequilibrium state. These results highlight that a rather simple avenue of changing the PNC preparation conditions, for example, the polymer concentration in solution, could strongly affect their macroscopic properties by trapping them in a deep metastable state.

We conclude that a good polymer chain packing in the interfacial region leads to such a substantial increase in mechanical properties. The approach presented here is unique in its simplicity and could be applicable to various types of glassy PNCs with attractive interaction. Rather than changing a series of parameters (e.g., NP size and loading, temperature, molecular weight, polymer chain rigidity, polymer—NP interaction, and chain stretching), simply tuning the polymer concentration in the precursor solution also can provide handles to control the interfacial region and mechanical

properties of glassy PNCs. However, these results cannot be generalized to other PNCs, where polymer—NP interactions are either neutral or repulsive in nature. Significant NP aggregation might play a major role in properties of these PNCs.

#### MATERIALS AND METHODS

Synthesis and Characterization of PNCs. PNCs were prepared by blending SiO<sub>2</sub> NPs with P2VP. SiO<sub>2</sub> NPs were synthesized in ethanol by a modified Stöber method. <sup>39,40</sup> NPs were characterized by SAXS in ethanol at 0.7 vol % dilution. The scattered intensity revealed a log-normal size distribution, with a radius of  $R_{NP} = 8.0$  nm and polydispersity ( $\sigma_0$ ) equal to 0.18. After synthesis, the NP suspension was passed through a 0.2  $\mu$ m PTFE filter to remove large aggregates and impurities, with a final NP concentration of 18.5 mg/mL determined from the mass of dried SiO<sub>2</sub> NPs in the suspension volume. P2VP with a molecular weight of 400 kg/mol and a polydispersity index of 1.07 was purchased from Scientific Polymer Products Inc. and used as received. PNCs were prepared from several solution concentrations. First, 0.20 g of P2VP was dissolved in ethanol and stirred at room temperature for  $\sim$ 2 h with a magnetic stirring bar. Four different ethanol volumes of 2.8, 12.8, 22.8, and 192.8 mL were selected to dissolve P2VP, accordingly, the polymer concentrations in solutions were calculated as 20, 10, 6.7, and 1 mg/mL. Then, 7.2 mL of SiO<sub>2</sub> NP suspension was added into the above-prepared polymer solutions in a dropwise manner under stirring and then continually stirred for ~12 h to ensure good dispersion of NPs. Each sample has a constant NP to polymer weight ratio. After mixing, the solution was then poured into a Teflon dish to first dry under a hood for ~24 h and then dried in a vacuum oven at 373 K for 2 days to ensure removal of the solvent from the PNCs (see the thermogravimetric data in the Supporting Information). In addition, prior to characterization, the samples were dried for 12 h at T = 423 K to remove the residual solvent and adsorbed moisture. The resulting PNCs are designated as PNC-20 mg/mL, PNC-10 mg/mL, PNC-6.7 mg/mL, and PNC-1 mg/mL, respectively. The pure polymer matrix was prepared in ethanol at a concentration of 10 mg/mL and then dried in the same way as PNCs.

The volume fractions of SiO<sub>2</sub> NPs ( $\varphi_{NP}$ ) in PNCs (Table 1) were determined by thermogravimetric analysis (TGA, TA Instruments, Discovery Q50) based on the weight loss and the following equation

$$\varphi_{\rm NP} = \frac{\frac{m_{\rm NP}}{\rho_{\rm NP}}}{\frac{m_{\rm NP}}{\rho_{\rm NP}} + \frac{m_{\rm P2VP}}{\rho_{\rm P2VP}}} \times 100\% \tag{1}$$

here  $\rho_{\rm NP}=2.406~{\rm g/cm^3}$  is the density of SiO $_2$  NPs,  $\rho_{\rm P2VP}=1.224~{\rm g/cm^3}$  is the P2VP density,  $m_{\rm NP}$  and  $m_{\rm P2VP}$  are the mass fraction of SiO $_2$  NPs and P2VP, respectively. Specifically, the PNCs were heated from ambient temperature to 873 K at a heating rate of 20 K/min under air. The mass densities of neat P2VP and PNCs were measured using a gas pycnometer (Micromeritics AccuPyc II 1340) using helium gas at 293 K and 1 atm pressure. The density of SiO $_2$  NPs was taken from our earlier publications.  $^{9,31,32}_{31,32}$  SAXS spectra of SiO $_2$  NPs/ethanol in a capillary, an empty capillary, and free standing films of neat P2VP and PNCs were collected using a Xenocs Xeuss 3.0 instrument with a beam wavelength  $\lambda=1.54$  Å. Prior to SAXS measurements, all samples were annealed at 433 K for ~2 h the same as BDS measurements. The average interparticle surface-to-surface distance ( $d_{\rm IPS}$ ) is estimated by assuming cubic packing of NPs in PNCs as follows,  $^{41}_{}$  and values are listed in Table 1.

$$d_{\rm IPS} = \left( \left( \frac{3\varphi_{\rm NP}}{4\pi} \right)^{-1/3} - 2 \right) \times R_{\rm NP}$$
 (2)

USAXS data were collected for samples PNC-1 mg/mL, PNC-20 mg/mL, and polymers on a USAXS instrument at APS sector 9ID.  $^{43}$  X-ray beam energy was 21 keV, and the data collection time was 90 s with a beam size of 0.8  $\times$  0.8 mm. Data were corrected for all

instrument effects, and intensity was calculated on an absolute scale [1/cm]. The results of USAXS measurements are presented in the Supporting Information.

Broadband Dielectric Spectroscopy. BDS measurements were conducted on a Novocontrol Concept-80 system with an Alpha-A impedance analyzer and a Quatro Cryosystem temperature controller with a stability of  $\pm 0.1$  K. The complex dielectric permittivity,  $\varepsilon^*(\omega)$ =  $\varepsilon'(\omega)$  –  $i\varepsilon''(\omega)$ , was collected in a frequency range of  $10^{-2}$  to  $10^{7}$ Hz ( $\omega = 2\pi f$ ) at temperatures from 433 to 143 K. Prior to BDS tests, all samples were heated at ~400-420 K to form a thin film with a typical thickness of ~0.1-0.2 mm, followed by annealing in a vacuum oven at 373 K for 2 days. The resulting thin films were sandwiched between two disk-shaped gold-coated electrodes with diameters of 10 and 20 mm, respectively. The samples were further annealed at 433 K for ~2 h in a dielectric sample chamber under nitrogen flow to ensure both real and imaginary parts of permittivity became constant for any given frequency. Then, the samples were measured at temperatures from 433 K with an interval of 5 K down to 383 K and then with an interval of 10 K down to 143 K. After that, the samples were heated up to room temperature to verify possible thickness changes. A thermal equilibration of 20 min was performed prior to each temperature measurement (see Section S10 in the Supporting Information for additional results related to time-dependent changes). To remove any possible artifacts coming from the measurements (e.g., thickness changes of samples),  $\varepsilon'(\omega)$  and  $\varepsilon''(\omega)$  of PNCs were normalized to the high-frequency limit of the real part measured at the lowest temperature of 143 K  $(\varepsilon_{\infty,143\mathrm{K}})$  using the following

$$\varepsilon'(\omega) = \frac{\varepsilon'_{\text{measured}}(\omega)}{\frac{\varepsilon_{\infty,143K}}{\varepsilon_{\infty,PNC}}}$$
(3)

$$\varepsilon''(\omega) = \frac{\varepsilon''_{\text{measured}}(\omega)}{\frac{\varepsilon_{\infty,143K}}{\varepsilon_{\infty,PNC}}}$$
(4)

where  $\varepsilon_{\infty, \text{PNC}} = (1 - \varphi_{\text{NP}}) \times \varepsilon_{\infty, \text{P2VP}} + \varphi_{\text{NP}} \times \varepsilon_{\infty, \text{NP}}$  was calculated based on a two-component heterogeneous model and taking  $\varepsilon_{\infty, \text{P2VP}} = 3.05$  and  $\varepsilon_{\infty, \text{NP}} = 3.9$  for the P2VP and silica permittivity values, respectively.

**Brillouin Light Scattering.** BLS spectra of the neat polymer and PNCs were measured using a tandem Fabry–Pérot interferometer in a transmission symmetric scattering geometry at a scattering angle of  $90^{\circ}$  and the laser wavelength  $\lambda_{\rm laser} = 532$  nm (Verdi from Coherent). The advantage of the symmetric scattering geometry is the compensation of the refractive index that enables the estimation of the sound velocity from the Brillouin peak frequency without knowledge of the materials' refractive index. The power of the incident laser beam was  $\sim 30$  mW. The BLS spectra for both LM and TM were measured. Prior to BLS measurements, all samples were first annealed at 433 K for  $\sim 2$  h the same as BDS and SAXS measurements, then sandwiched between two sapphire glass windows to ensure that the samples have parallel surfaces and a uniform thickness of  $\sim 1$  mm. The mirror distance in the tandem Fabry–Pérot interferometer was fixed to 5 mm.

#### ASSOCIATED CONTENT

#### Supporting Information

The Supporting Information is available free of charge at https://pubs.acs.org/doi/10.1021/acsapm.1c01623.

Calculation of the radius of gyration  $(R_g)$  and critical concentration  $(C^*)$ ; calculation of the distance between  $SiO_2$  NPs in solution; analysis of BDS spectra using ILM; estimate of mechanical properties using mechanical TPM and ILM; PCS results; ICFs; characteristics of  $SiO_2$  NPs and PNCs in solution; DSC analysis; reversing heat capacity and its derivative; representative plot of the LM from BLS; segmental relaxation; volume fraction of

the interfacial region presented as a function of polymer concentration; SCFT calculations; SCFT parameters for simulating the adsorption of P2VP chains from ethanol onto a single spherical nanoparticle; segment and solvent density profile; density profiles of loops, tails, and free segments near the spherical nanoparticle; segment and solvent density profiles for various strengths of the segment-solvent interaction parameter; additional thermogravimetric data and kinetic study data; comparison of the dielectric loss spectra; annealing time dependence of the segmental relaxation times and conductivity; USAXS data; analytical estimates of polymer adsorption onto a spherical nanoparticle; and the effect of segment-nanoparticle interaction energy strength on the number of adsorbed monomers of a chain (PDF)

#### AUTHOR INFORMATION

#### **Corresponding Authors**

Zhengping Zhou – Chemical Sciences Division, Physical Sciences Directorate, Oak Ridge National Laboratory, Oak Ridge, Tennessee 37831, United States; Oorcid.org/0000-0002-4706-5499; Email: zhouz@ornl.gov

Alexei P. Sokolov — Chemical Sciences Division, Physical Sciences Directorate, Oak Ridge National Laboratory, Oak Ridge, Tennessee 37831, United States; Department of Chemistry, University of Tennessee, Knoxville, Tennessee 37996, United States; orcid.org/0000-0002-8187-9445; Email: sokolov@utk.edu

#### Authors

Vera Bocharova — Chemical Sciences Division, Physical Sciences Directorate, Oak Ridge National Laboratory, Oak Ridge, Tennessee 37831, United States; orcid.org/0000-0003-4270-3866

Rajeev Kumar – Center for Nanophase Materials Sciences, Oak Ridge National Laboratory, Oak Ridge, Tennessee 37831, United States; © orcid.org/0000-0001-9494-3488

Anne-Caroline Genix — Laboratoire Charles Coulomb, Université de Montpellier, CNRS, Montpellier F-34095, France

Bobby Carroll – Department of Chemistry, University of Tennessee, Knoxville, Tennessee 37996, United States

Subarna Samanta – Department of Chemistry, University of Tennessee, Knoxville, Tennessee 37996, United States

Ivan Popov – Chemical Sciences Division, Physical Sciences Directorate, Oak Ridge National Laboratory, Oak Ridge, Tennessee 37831, United States

Amanda Young-Gonzales — Department of Chemistry, University of Tennessee, Knoxville, Tennessee 37996, United States

Alexander Kisliuk – Chemical Sciences Division, Physical Sciences Directorate, Oak Ridge National Laboratory, Oak Ridge, Tennessee 37831, United States

Seung Pyo Jeong — Chemical Sciences Division, Physical Sciences Directorate, Oak Ridge National Laboratory, Oak Ridge, Tennessee 37831, United States; orcid.org/0000-0002-3444-6129

Jan Ilavsky – Advanced Photon Source, Argonne National Laboratory, Argonne, Illinois 60439, United States

Complete contact information is available at: https://pubs.acs.org/10.1021/acsapm.1c01623

#### **Author Contributions**

Z.Z., V.B., and A.P.S. carried out and designed the experiments. R.K. performed the computer simulations. A.Y.-G. helped in the analysis of SAXS and BDS results. A.K. participated the BLS measurements. S.S., I.P., and A.Y.-G. helped in the fitting of BDS results. S.P.J. helped in the synthesis of silica NPs. J.I. performed USAXS experiments. All authors discussed the results and commented on the manuscript.

#### Notes

The authors declare no competing financial interest.

#### ACKNOWLEDGMENTS

This work was supported by the U.S. Department of Energy, Office of Science, Basic Energy Sciences, Materials Sciences and Engineering Division. S.S. acknowledges partial financial support from NSF (DMR-1904657) for some of the dielectric measurements and data analysis. Theory and simulations were a portion of this research was conducted at the Center for Nanophase Materials Sciences, which is a DOE Office of Science User Facility. This research used resources of the National Energy Research Scientific Computing Center (NERSC) and the Compute and Data Environment for Science (CADES) at the Lawrence Berkeley National Laboratory and the Oak Ridge National Laboratory, which are supported by the Office of Science of the U.S. Department of Energy under Contract no. DE-AC02-05CH11231 and DE-AC05-00OR22725, respectively. This research used resources of the Advanced Photon Source, a U.S. Department of Energy (DOE) Office of Science User Facility operated for the DOE Office of Science by Argonne National Laboratory under Contract no. DE-AC02-06CH11357.

#### REFERENCES

- (1) Balazs, A. C.; Emrick, T.; Russell, T. P. Nanoparticle Polymer Composites: Where Two Small Worlds Meet. *Science* **2006**, *314*, 1107–1110.
- (2) Podsiadlo, P.; et al. Ultrastrong and Stiff Layered Polymer Nanocomposites. *Science* **2007**, *318*, 80–83.
- (3) Mangal, R.; Srivastava, S.; Archer, L. A. Phase stability and dynamics of entangled polymer-nanoparticle composites. *Nat. Commun.* **2015**, *6*, 7198.
- (4) Kashiwagi, T.; Du, F.; Douglas, J. F.; Winey, K. I.; Harris, R. H.; Shields, J. R. Nanoparticle networks reduce the flammability of polymer nanocomposites. *Nat. Mater.* **2005**, *4*, 928–933.
- (5) Chen, H.-Y.; Lo, M. K. F.; Yang, G.; Monbouquette, H. G.; Yang, Y. Nanoparticle-assisted high photoconductive gain in composites of polymer and fullerene. *Nat. Nanotechnol.* **2008**, 3, 543–547.
- (6) Naskar, A. K.; Keum, J. K.; Boeman, R. G. Polymer matrix nanocomposites for automotive structural components. *Nat. Nanotechnol.* **2016**, *11*, 1026–1030.
- (7) Kinloch, I. A.; Suhr, J.; Lou, J.; Young, R. J.; Ajayan, P. M. Composites with carbon nanotubes and graphene: An outlook. *Science* **2018**, *362*, 547–553.
- (8) Kumar, S. K.; Benicewicz, B. C.; Vaia, R. A.; Winey, K. I. 50th Anniversary Perspective: Are Polymer Nanocomposites Practical for Applications? *Macromolecules* **2017**, *50*, 714–731.
- (9) Genix, A.-C.; et al. Enhancing the Mechanical Properties of Glassy Nanocomposites by Tuning Polymer Molecular Weight. ACS Appl. Mater. Interfaces 2018, 10, 33601–33610.
- (10) Cheng, S.; et al. Big Effect of Small Nanoparticles: A Shift in Paradigm for Polymer Nanocomposites. *ACS Nano* **2017**, *11*, 752–759.

- (11) Schadler, L. S.; Kumar, S. K.; Benicewicz, B. C.; Lewis, S. L.; Harton, S. E. Designed Interfaces in Polymer Nanocomposites: A Fundamental Viewpoint. *MRS Bull.* **2011**, *32*, 335–340.
- (12) Starr, F. W.; Douglas, J. F.; Meng, D.; Kumar, S. K. Bound Layers "Cloak" Nanoparticles in Strongly Interacting Polymer Nanocomposites. *ACS Nano* **2016**, *10*, 10960–10965.
- (13) Zhang, W.; Starr, F. W.; Douglas, J. F. Collective Motion in the Interfacial and Interior Regions of Supported Polymer Films and Its Relation to Relaxation. *J. Phys. Chem. B* **2019**, *123*, 5935–5941.
- (14) Yang, S.; Akcora, P. Deformation of Chemically Heterogeneous Interfacial Layers of Polymer Nanocomposites. *ACS Macro Lett.* **2019**, *8*, 1635–1641.
- (15) Bailey, E. J.; Winey, K. I. Dynamics of polymer segments, polymer chains, and nanoparticles in polymer nanocomposite melts: A review. *Prog. Polym. Sci.* **2020**, *105*, 101242.
- (16) Cheng, S.; et al. Unexpected Molecular Weight Effect in Polymer Nanocomposites. *Phys. Rev. Lett.* **2016**, *116*, 038302.
- (17) Holt, A. P.; et al. Dynamics at the Polymer/Nanoparticle Interface in Poly(2-vinylpyridine)/Silica Nanocomposites. *Macromolecules* **2014**, 47, 1837–1843.
- (18) Carroll, B.; Cheng, S.; Sokolov, A. P. Analyzing the Interfacial Layer Properties in Polymer Nanocomposites by Broadband Dielectric Spectroscopy. *Macromolecules* **2017**, *50*, 6149–6163.
- (19) Cheng, S.; et al. Interfacial Properties of Polymer Nanocomposites: Role of Chain Rigidity and Dynamic Heterogeneity Length Scale. *Macromolecules* **2017**, *50*, 2397–2406.
- (20) Cheng, S.; et al. Revealing spatially heterogeneous relaxation in a model nanocomposite. *J. Chem. Phys.* **2015**, *143*, 194704.
- (21) Holt, A. P.; et al. Controlling Interfacial Dynamics: Covalent Bonding versus Physical Adsorption in Polymer Nanocomposites. *ACS Nano* **2016**, *10*, 6843–6852.
- (22) Cheng, S.; Carroll, B.; Bocharova, V.; Carrillo, J.-M.; Sumpter, B. G.; Sokolov, A. P. Focus: Structure and dynamics of the interfacial layer in polymer nanocomposites with attractive interactions. *J. Chem. Phys.* **2017**, *146*, 203201.
- (23) Carrillo, J.-M. Y.; Cheng, S.; Kumar, R.; Goswami, M.; Sokolov, A. P.; Sumpter, B. G. Untangling the Effects of Chain Rigidity on the Structure and Dynamics of Strongly Adsorbed Polymer Melts. *Macromolecules* **2015**, *48*, 4207–4219.
- (24) Wu, D.; Weiblen, D. G.; Ozisik, R.; Akcora, P. Local Viscosity of Interfacial Layers in Polymer Nanocomposites Measured by Magnetic Heating. ACS Appl. Polym. Mater. 2020, 2, 5542–5549.
- (25) Gong, S.; Chen, Q.; Moll, J. F.; Kumar, S. K.; Colby, R. H. Segmental Dynamics of Polymer Melts with Spherical Nanoparticles. *ACS Macro Lett.* **2014**, *3*, 773–777.
- (26) Jouault, N.; Zhao, D.; Kumar, S. K. Role of Casting Solvent on Nanoparticle Dispersion in Polymer Nanocomposites. *Macromolecules* **2014**, *47*, 5246–5255.
- (27) Zhao, D.; Schneider, D.; Fytas, G.; Kumar, S. K. Controlling the Thermomechanical Behavior of Nanoparticle/Polymer Films. *ACS Nano* **2014**, *8*, 8163–8173.
- (28) Carroll, B.; et al. Diffusion of Sticky Nanoparticles in a Polymer Melt: Crossover from Suppressed to Enhanced Transport. *Macromolecules* **2018**, *51*, 2268–2275.
- (29) Füllbrandt, M.; Purohit, P. J.; Schönhals, A. Combined FTIR and Dielectric Investigation of Poly(vinyl acetate) Adsorbed on Silica Particles. *Macromolecules* **2013**, *46*, 4626–4632.
- (30) Popov, I.; et al. Strong Reduction in Amplitude of the Interfacial Segmental Dynamics in Polymer Nanocomposites. *Macromolecules* **2020**, *53*, 4126–4135.
- (31) Bocharova, V.; et al. Addition of Short Polymer Chains Mechanically Reinforces Glassy Poly(2-vinylpyridine)-Silica Nanoparticle Nanocomposites. *ACS Appl. Nano Mater.* **2020**, *3*, 3427–3438.
- (32) Cheng, S.; et al. Unraveling the Mechanism of Nanoscale Mechanical Reinforcement in Glassy Polymer Nanocomposites. *Nano Lett.* **2016**, *16*, 3630–3637.
- (33) Hong, L.; Begen, B.; Kisliuk, A.; Alba-Simionesco, C.; Novikov, V. N.; Sokolov, A. P. Pressure and density dependence of the boson

- peak in polymers. Phys. Rev. B: Condens. Matter Mater. Phys. 2008, 78, 134201.
- (34) van der Poel, C. On the rheology of concentrated dispersions. *Rheol. Acta* **1958**, *1*, 198–205.
- (35) Hashin, Z. Thermoelastic properties of particulate composites with imperfect interface. *J. Mech. Phys. Solids* **1991**, 39, 745–762.
- (36) Maurer, F. H. J. An Interlayer Model to Describe the Physical Properties of Particulate Composites; Springer Netherlands, 1990.
- (37) Zhou, Y.; et al. Bridging-Controlled Network Microstructure and Long-Wavelength Fluctuations in Silica-Poly(2-vinylpyridine) Nanocomposites: Experimental Results and Theoretical Analysis. *Macromolecules* **2020**, *53*, 6984–6994.
- (38) Hall, L. M.; Schweizer, K. S. Many body effects on the phase separation and structure of dense polymer-particle melts. *J. Chem. Phys.* **2008**, 128, 234901.
- (39) Kamiya, H.; Suzuki, H.; Kato, D.; Jimbo, G. Densification of Alkoxide-Derived Fine Silica Powder Compact by Ultra-High-Pressure Cold Isostatic Pressing. *J. Am. Ceram. Soc.* **1993**, *76*, 54–64.
- (40) Stöber, W.; Fink, A.; Bohn, E. Controlled growth of monodisperse silica spheres in the micron size range. *J. Colloid Interface Sci.* **1968**, 26, 62–69.
- (41) Wu, S. Phase structure and adhesion in polymer blends: A criterion for rubber toughening. *Polymer* **1985**, *26*, 1855–1863.
- (42) Sinogeikin, S.; et al. Brillouin spectrometer interfaced with synchrotron radiation for simultaneous x-ray density and acoustic velocity measurements. *Rev. Sci. Instrum.* **2006**, *77*, 103905.
- (43) Ilavsky, J.; Zhang, F.; Andrews, R. N.; Kuzmenko, I.; Jemian, P. R.; Levine, L. E.; Allen, A. J. Development of combined microstructure and structure characterization facility forin situandoperandostudies at the Advanced Photon Source. *J. Appl. Crystallogr.* **2018**, *51*, 867–882.

### **□** Recommended by ACS

#### Collective Nanoparticle Dynamics Associated with Bridging Network Formation in Model Polymer Nanocomposites

Benjamin M. Yavitt, Tadanori Koga, et al.

JUNE 15, 2021 ACS NANO

READ 🗹

## Structure, Dynamics, and Mechanical Properties of Polyimide-Grafted Silica Nanocomposites

Yu Lin, Guozhang Wu, et al.

MARCH 04, 2019

THE JOURNAL OF PHYSICAL CHEMISTRY C

READ 🗹

#### Effect of Nanoparticle Organization on Molecular Mobility and Mechanical Properties of Polymer Nanocomposites

Frantisek Ondreas, Josef Jancar, et al.

AUGUST 13, 2019 MACROMOLECULES

READ **C** 

#### Chain and Segmental Dynamics in Polymer-Nanoparticle Composites with High Nanoparticle Loading

Emily Y. Lin, Robert A. Riggleman, et al.

JUNE 09, 2021

MACROMOLECULES

READ 🗹

Get More Suggestions >